

Models for Solar Abundance Stars with Gravitational Settling and Radiative Accelerations: Application to M 67 and NGC 188

G. Michaud, O. Richard¹, & J. Richer

Département de Physique, Université de Montréal, Montréal, PQ, H3C 3J7

michaudg@astro.umontreal.ca, Olivier.Richard@graal.univ-montp2.fr,
jacques.richer@umontreal.ca

and

Don A. Vandenberg

*Department of Physics & Astronomy, University of Victoria, P.O. Box 3055, Victoria, BC,
V8W 3P6, Canada*

davb@uvvm.uvic.ca

ABSTRACT

Evolutionary models taking into account radiative accelerations, thermal diffusion, and gravitational settling for 28 elements, including all those contributing to OPAL stellar opacities, have been calculated for solar metallicity stars of 0.5 to 1.4 M_{\odot} . The Sun has been used to calibrate the models. Isochrones are fitted to the observed color-magnitude diagrams (CMDs) of M 67 and NGC 188, and ages of 3.7 and 6.4 Gyr are respectively determined. Convective core overshooting is *not* required to match the turnoff morphology of either cluster, including the luminosity of the gap in M 67, because central convective cores are larger when diffusive processes are treated. This is due mainly to the enhanced helium and metal abundances in the central regions of such models. The observation of solar metallicity open clusters with ages in the range 4.8–5.7 Gyr would further test the calculations of atomic diffusion in central stellar regions: according to non-diffusive isochrones, clusters should not have gaps near their main-sequence turnoffs if they are older than ≈ 4.8 Gyr, whereas diffusive isochrones predict that gaps should persist up to ages of ≈ 5.7 Gyr.

Surface abundance isochrones are also calculated. In the case of M 67 and NGC 188, surface abundance variations are expected to be small. Abundance differences between stars of very similar T_{eff} are expected close to the turnoff, especially for elements between P and Ca. Moreover, in comparison with the results obtained for giants, small generalized underabundances are expected in main-sequence stars. The lithium to

¹GRAAL UMR5024, Université Montpellier II, CC072, Place E. Bataillon, 34095 Montpellier Cedex, France

beryllium ratio is discussed briefly and compared to observations. The inclusion of a turbulent transport parametrization that reduces surface abundance variations does not significantly modify computed isochrones.

Subject headings: convection — diffusion — color-magnitude diagrams (HR diagrams)
— open clusters: general — open clusters (M 67, NGC 188) — stars: general

October 29, 2018

1. ASTROPHYSICAL CONTEXT

The open clusters M 67 and NGC 188 have about the solar metallicity, bracket the solar age, and have turnoff stars only a few hundred degrees hotter than the Sun. As such, they are interesting testing grounds for the effects of atomic diffusion on age determinations and surface abundances, since, in the case of the Sun, there is now ample evidence from heliosismology that atomic diffusion has reduced the surface He abundance (Guzik & Cox 1992; Guzik & Cox 1993; Christensen-Dalsgaard et al. 1993; Proffitt 1994; Bahcall et al. 1995; Guenther et al. 1996; Richard et al. 1996; Brun et al. 1999). Indeed, diffusive processes presumably also cause small underabundances of metals in the Sun: these are caused mainly by gravitational settling, but are also modified by radiative accelerations (g_{rad}), which are predicted to be especially important at the end of the main-sequence phases of solar-type stars (Turcotte et al. 1998). What abundance anomalies are then to be expected in the turnoff stars of M 67, which are ~ 400 K hotter than the Sun (Hobbs & Thorburn 1991), and in those of NGC 188, which are ~ 100 K hotter (Hobbs et al. 1990)? As the cluster turnoff stars are expected to have smaller surface convection zones, they may show larger effects of atomic diffusion than the Sun.

On the other hand, since the radius and age of the Sun are used to calibrate the mixing length and assumed initial He abundance, this normalization may eliminate the effects of diffusion on age determinations. Whereas an $\approx 10\%$ reduction in age at a given turnoff luminosity — compared with the predictions of models that neglect diffusion — was derived by Vandenberg et al. (2002) from the diffusive models for Population II stars computed by Richard et al. (2002), it is not clear that a similar reduction should be expected in the case of Pop. I stars. In addition, there may be some important differences in the morphologies of the diffusive and non-diffusive isochrones in the age range where a transition is made between isochrones that have a gap near the main-sequence turnoff and those which do not. One naively expects that both the sizes of convective cores in models for main-sequence stars of a given mass, and the predicted mass marking the transition between stars that have convective and radiative cores on the main sequence, will depend (to some extent) on whether or not diffusive processes are treated. (For instance, the concomitant increase in opacity with the settling of Fe in the cores of stars would tend to enhance convective instability.)

In this regard, we note that the first studies of NGC 188 (Sandage 1962; Eggen & Sandage

1969) concluded that it has a gap near the top of its main-sequence on the $(V, B - V)$ -diagram reminiscent of that seen in M67. McClure & Twarog (1977) carried out a statistical test of the photographic photometry that they obtained for the same cluster, and confirmed the existence of the gap in the color-magnitude diagram (CMD) that was constructed for stars within Ring I on Sandage’s original finder chart. Curiously, no statistically significant evidence for a gap was found if their CMD included stars in Sandage’s Ring II; but McClure & Twarog concluded that contamination by field stars was almost certainly much more severe in the outer ring and that, if it were possible to remove the field stars, “the gap would be obvious”. The proper-motion membership study of Dinescu et al. (1996) does not shed any light on this problem (because of the very large scatter in their CMD fainter than $V = 15$: the gap is located at $V \approx 15.5$ according to McClure & Twarog). However Platais et al. (2003) provide a well defined CMD down to $V = 20$, with no indication of a turnoff gap.

Because there is no obvious indication of a gap in subsequent CMDs for NGC 188 (e.g., Kaluzny 1990; Caputo et al. 1990; Sarajedini et al. 1999), and because the best-fitting isochrones for current best estimates of the cluster distance and reddening do not predict a gap at the turnoff M_V (see the aforementioned papers), its existence is considered by many to be quite doubtful. However, the models that have been compared with the cluster CMD have not taken gravitational settling and radiative accelerations into account. If it were shown that diffusive isochrones do, in fact, predict a main-sequence gap, not necessarily for NGC 188 but for any range in age where a gap is not predicted by models that neglect diffusion, this would be an important development that would motivate a search for open clusters within the requisite age range to further test our understanding of stellar physics.

There are many other questions that need to be addressed. In particular, does the same turbulence parametrization that Richard et al. (2002) used, in conjunction with diffusion physics, to explain the Li abundances in field halo stars, also lead to good agreement between the predicted and observed Li abundances in solar-type stars, as well as in those that were in the Li gap at the age of the Hyades (Balachandran 1995)? The surface abundances of Li in M67 solar-type stars (see Fig. 7 of Martín et al. 2002) vary from star to star at a given T_{eff} , which suggests that mixing processes below the surface convection zone vary from star to star at a given mass. Did the turbulence differ only in the early stellar histories of the cluster stars or is it still different between one solar twin and another? To what extent is this confirmed by abundance anomalies of other species and do such anomalies affect theoretical isochrones? Furthermore, what abundance anomalies of Fe, Li, C, and O could be caused by diffusion and are they observed (Barrett et al. 2001)?

In NGC 188, the surface Li abundance in solar-type stars appears to be consistent with a single-valued function of T_{eff} just as in the Hyades (see Randich et al. 2003). Furthermore, even though NGC 188 is older than M67 by $\sim 2\text{--}3 \times 10^9$ years (e.g., Sarajedini et al. 1999), the Li abundance in its G-type stars is comparable with the largest abundances measured in M67 stars having similar colors/temperatures. Could a simpler model account for the Li observations in the Hyades and NGC 188 than in M67? Pre-main-sequence evolution could be largely responsible for

the Li destruction in the Hyades and NGC 188 (see, for instance, Proffitt & Michaud 1989; Piau & Turck-Chièze 2002). Finally, we note that the relative abundances of Li and Be along the subgiant branch of M 67 has been evaluated in models including gravitational settling by Sills & Deliyannis (2000). However, what are the ratios of the Li and Be abundances to be expected from diffusion if g_{rad} are also taken into account?

In this paper, after a very brief description of the calculations in §2, the chemical composition expected on the surfaces of stars of M 67 and NGC 188 will be discussed in §3.1 and Li/Be ratios in §3.2. The effect of atomic diffusion on central convective cores is analyzed in detail in §3.3. The effect of diffusion on isochrones is discussed in §4 and these results are applied to M 67 and NGC 188 in §5. The main conclusions are summarized in §6. Throughout this paper the emphasis is on calculations in the presence of atomic diffusion and, in some cases, of turbulent transport with the same parametrization as used for Pop II stars by Richard et al. (2002). The discussion of potential star-to-star variations of turbulent transport to explain Li abundance spread at a given T_{eff} is left to a paper in preparation.

2. CALCULATIONS

The models were calculated as described by Turcotte et al. (1998) and Richard et al. (2001). They were assumed to be chemically homogeneous on the pre-main sequence with a solar abundance mix, and relative concentrations as defined in Table 1 of Turcotte et al. (1998). The radiative accelerations are from Richer et al. (1998) with the correction for redistribution from Gonzalez et al. (1995) and LeBlanc et al. (2000). The atomic diffusion coefficients were taken from Paquette et al. (1986) (see also Michaud & Proffitt 1993). In all cases, the Krishna Swamy T - τ relation (Krishna Swamy 1966) was used to derive the outer boundary condition for the pressure that is needed to construct stellar models. Semiconvection was included as described in Richard et al. (2001), following Kato (1966), Langer et al. (1985), and Maeder (1997).

In Turcotte et al. (1998), the solar luminosity and radius at the solar age were used to determine the value of α , the ratio of the mixing length to the pressure scale-height in the usual mixing-length theory (MLT) of convection, and of Y_0 , the He concentration in the zero-age Sun. The value of Y_0 mainly affects the luminosity while α primarily determines the radius, through the depth of the surface convection zone. The required value of α was found to be slightly larger in the diffusive, than in the non-diffusive, models because an increased value of α is needed to compensate for the settling of He and the metals from the surface convection zone. The increase in α in the diffusion models of the Sun is thus determined by the settling that occurs immediately below the solar surface convection zone.

The value of α and the initial values of Y_0 and Z_0 that were adopted in each of the three series of models computed for this study are given in Table 1, together with the accuracy with which they represent the solar properties at the solar age. We did not force convergence as precisely

as in Turcotte et al. (1998), but the convergence should suffice for the purposes of this paper. The model with atomic diffusion only is calculated using the same values of Y_0 , Z_0 , and α as in Turcotte et al. (1998), even though small changes were since made to the code, such as a better treatment of some interaction terms in the diffusion equations for the various species. (This is what has caused a slight degradation of the convergence criteria.) For the non-diffusive case, the values of Y_0 , Z_0 , and α tabulated by Turcotte et al. (1998) (Model B of their Table 2) were calculated using tables of mean opacities while, here, the monochromatic opacities were used even for models without diffusion. This causes small differences in the central regions of the solar model where CNO abundance variations modify the opacity — leading to slight differences in our value of α (see Table 1) compared with that used in model B of Turcotte et al. (1998).

One series of models was calculated with the same turbulent transport parametrization, labeled T6.09, that was found to minimize the surface Li abundance changes in Pop. II field stars (see Richard et al. 2002 for both the definition of this turbulent transport parametrization and its justification). As may be seen from Fig. 6 of Richard et al. (2002), that turbulent transport coefficient approximately equals the He atomic diffusion coefficient at $\log T = 6.3$ and diminishes rapidly as T increases further. Because this is the temperature close to the bottom of the solar surface convection zone, this level of turbulent transport does not affect solar models significantly. We have, in fact, verified that the same values of Y_0 , Z_0 , and α are obtained for the calibrated solar models that allow for only atomic diffusion, on the one hand, and atomic diffusion plus T6.09 turbulence, on the other. Since, furthermore, it is the effect of adding turbulence to models with atomic diffusion that we wish to study, the models with turbulence must have the same Y_0 and α as those with atomic diffusion only.

3. EVOLUTIONARY MODELS

In Figure 1 are shown, for a few of the calculated models, the time dependence of T_{eff} as well as of the depth of the surface and central convection zones. The data were taken from some of the models without diffusion (top row) and from some with atomic diffusion (bottom row). The surface convection zone mixes to the surface the abundances that are modified by atomic diffusion below the fully mixed outer layers. The time dependence of the depth of the surface convection zone determines the time dependence of the depth of the region where element separation occurs. In these models, the smallest convection zones (in terms of the amount of mass that they contain) occur early in the evolution and for a brief period just past the turnoff. This is different from the stars in low-metallicity Pop. II globular clusters in which the mass in the surface convection zone decreases throughout the main-sequence phase (see Fig. 1 of Richard et al. 2002).

3.1. Chemical composition

Figure 2 illustrates the variation in the surface abundances of several species as a function of T_{eff} at 3.7 Gyr, which is our estimate of the age of M 67 (see §5 below). These “surface abundance isochrones” were calculated for an additional 19 species, but only representative ones are shown: the other loci bear considerable similarity to those that have been plotted. The corresponding g_{rad} are illustrated in Figure 3 for B, Mg, P, Ti, Fe, and Ni. (The g_{rad} of He, Li, and Be are negligible in 1.3 M_{\odot} models.)

The surface abundances of ^3He and LiBeB are affected by both diffusion processes and nuclear reactions. The effect of nuclear reactions on the surface abundances of these elements becomes evident during the evolution of a star on the subgiant branch when dredge-up occurs. Overabundances of ^3He are predicted to appear as the star reaches $T_{\text{eff}} \approx 5400$ K (the temperature where the surface abundance isochrone becomes nearly vertical in Fig. 2). At this point in the star’s evolution, the bottom of the surface convection zone reaches down to regions where ^3He has a concentration maximum produced during the main–sequence stage (Iben 1965). For LiBeB, underabundances are expected at $T_{\text{eff}} \lesssim 5800$ K for Li and Be and $\lesssim 5600$ K for B (see Fig. 2): this occurs as the bottom of the surface convection zone reaches the regions where Li, Be, and B burn. The other abundance variations are caused by atomic diffusion.

In the model with atomic diffusion only, the surface abundance variations as a function of time are directly related to the depth of the surface convection zone (see Fig. 1): overabundances normally appear when $g_{\text{rad}} \geq g$ immediately below the surface convection zone. When the reverse is true, underabundances generally appear at the surface. The detailed results may be understood by remembering that, for those elements whose g_{rad} is small, the surface abundance decreases approximately as

$$\exp(-t/\theta) \tag{1}$$

where

$$\theta \simeq 2.3 \times 10^{11} (\Delta M / M_{\odot})^{0.545} \text{yr} \tag{2}$$

(for helium, with similar expressions for other species; see Michaud 1977). The precise value of the multiplying constant varies slightly with stellar mass, but more so with the atomic weight of each element and its charge¹. When θ is smaller than the age of the star, the abundance reached is a very sensitive function of the mixed mass.

The g_{rad} for B below the surface convection zone (see Fig. 3) is always smaller than gravity by at least a factor of two. Consequently, it has no more than a small effect (if any) on the boron concentration, which is mainly determined by gravitational settling until the bottom of the surface convection zone reaches the temperature where B burns.

¹In this paper, ΔM always represents the mass of the spherical shell *outside* a certain radius. Furthermore, in the above equation, this mass is assumed to be mixed (for instance, by convection).

The Mg abundance has a T_{eff} variation typical of species from O to Si: it is caused by g_{rad} (see Fig. 3) being much smaller than gravity below the surface convection zone, throughout the evolution of the stars in the relevant mass range. Elements from O to Si have g_{rad} with a similar $\log \Delta M/M_*$ dependence². All of these elements settle by gravitation below the surface convection zone and they have the largest underabundances at the end of the main–sequence phase. The underabundances are larger in the more massive stars because they have smaller surface convection zones (see Fig. 1).

P and Ti represent all elements between P and Ti (except for S, which is more like Mg). Their g_{rad} are slightly larger than gravity for a significant mass interval below the convection zone (see Fig. 3). The mass interval where g_{rad} is large varies from P to Ti. As the atomic number of the species increases, the larger values of g_{rad} shift to a greater depth. Very small overabundances may appear at the turnoff, but at a later epoch only in the more massive stars considered here. For most species, the effect of g_{rad} is merely to reduce the expected underabundances in the hotter stars.

Fe is representative of species of the Cr, Mn, Fe group. For all of them, g_{rad} is continuously smaller than gravity below the surface convection zone, but not by as large a factor as for Mg. Consequently, the predicted underabundances are not as large either. Finally, Ni is supported below the convection zone in the hotter stars considered.

In the presence of T6.09 turbulence, one expects underabundances of the metals at the $\sim 6\%$ level in stars between 4000 and 5000 K, progressively increasing to $\sim 12\%$ in stars of 6000 K. Only underabundances are predicted because the T6.09 turbulence mixes deep enough in the star (down to $\log \Delta M/M_* \simeq -2$) for g_{rad} never to play a dominant role. The g_{rad} still limit the underabundances of a number of species and, in particular, of Ti, as may be seen in Figure 2.

Similar results are shown in Figure 4 at the epoch corresponding to the age determined below for NGC 188, 6.4 Gyr. The abundance anomalies are larger at a given T_{eff} than those 2.7 Gyr earlier because of the longer time available for gravitational settling (Eq. 1). However, the stars with the largest T_{eff} at 3.7 Gyr have, at 6.4 Gyr, evolved away from the main sequence. They were the ones with the largest spread of anomalies of P, Fe, and Ni, at a given T_{eff} , in Fig. 2. The spread of abundance anomalies at the turnoff in Fig. 4 is much smaller due to the reduced importance of g_{rad} : only for Ti is the effect of g_{rad} still clearly visible. Similarly, at that age, T6.09 turbulence has very little effect since surface convection zones extend to $T \simeq 10^6$ K or ~ 10 times deeper than at 3.7 Gyr (see Fig. 1).

3.2. The Li/Be ratio in M 67

Sills & Deliyannis (2000) have calculated the Li/Be abundance ratio with a number of evolu-

²To see the variation of all g_{rad} with T , reference may be made to Fig. 1 in the study by Richer et al. (1998).

tionary models that included either turbulent transport, or atomic diffusion, or no transport process (dubbed *standard models*) and have presented a comparison of the different results in their Fig. 5. They used these results to determine the relative importance of those transport processes. In their models with atomic diffusion only, they obtain approximately a factor of 100 reduction of the Be abundance at the same time as a factor of 30 reduction of the Li abundance or $X(\text{Be}) \sim [X(\text{Li})]^{4/3}$. This is to be compared to the results shown on Figure 5 of this paper. On the leg of the isochrone corresponding to main–sequence stars, one has $X(\text{Be}) \sim [X(\text{Li})]^{4/5}$ while on the leg corresponding to subgiants, one has $X(\text{Be}) \sim X(\text{Li})$. Combining the two segments would give approximately $X(\text{Be}) \sim [X(\text{Li})]^{1/2}$ but with a large dispersion which is in agreement with the Li/Be ratios observed in field stars and discussed by Sills & Deliyannis (2000). Our results for the diffusion models are very different from theirs probably because of our more complete description of atomic diffusion processes.

Observations of Li and Be in M 67 were recently made by Randich et al. (2002) and their Li/Be ratios are also plotted on Figure 5. Some of their stars have V magnitudes that correspond to stars just before turnoff while others are slightly above it. Four of the five observed points are compatible with the model that includes only atomic diffusion processes. Given the error bars, the agreement could be considered satisfactory, however the star with the smallest Be abundance (S988) has a magnitude corresponding to pre–turnoff stars and so should not be on that segment of the curve.

One may also note that the original Li abundance used in these calculations (see Fig. 5) is smaller than usually believed to be appropriate in young solar metallicity clusters. This may however be affected by pre–main–sequence burning (see, for instance, Proffitt & Michaud 1989; Piau & Turck-Chièze 2002) which was neglected in this paper. Explaining the range of Li abundances observed in cluster and field stars requires a discussion of processes competing with atomic diffusion. This is outside the scope of the present paper but will be part of a paper in preparation.

3.3. Central convective cores and semiconvection

One of the consequences of the use of diffusive models is to modify the size of the central convective core (see Fig. 1), which will be seen in §4 to have a significant impact on the shape of temperature–luminosity isochrones. The convective core is larger in the diffusive models of a given mass than in those that neglect diffusion: 10% larger at $1.3 M_{\odot}$, 20% at $1.2 M_{\odot}$. Moreover, while the lowest mass *non-diffusive* model with a convective core is that for $1.14 M_{\odot}$, the lowest mass *diffusive* model with a convective core has a mass of $1.097 M_{\odot}$. This difference may be understood by studying the central properties of $1.1 M_{\odot}$ models. Three different models are compared in Figure 6; (i) our standard model with diffusion, (ii) that without diffusion, and (iii) one with the diffusion of He but without the diffusion of metals³.

³Note that, only for this discussion, do we consider a model with the diffusion of He but not of the metals.

The difference between the models with, and without, diffusion originates from metallicity and He abundance variations. Because of the normalization to the current properties of the Sun (see Turcotte et al. 1998), the initial Y (Y_0) is 3% larger in the solar model with diffusion than in the one without diffusion. On the other hand, in order to have the observed value of the ratio of surface metals to hydrogen (Z_\odot/X_\odot) at the solar age, the initial value of Z (Z_0) must be about 13% larger in the original solar model with diffusion than in the one without diffusion — in order to compensate appropriately for the effects of atomic diffusion during solar evolution (see Tables 2 and 6 of Turcotte et al. 1998). Consequently, our series of non-diffusive models have smaller Y_0 and Z_0 than our series of diffusive models (see Table 1). During the evolution, the central values of Y and Z are further increased by 3% to 4% by diffusion processes. At an age of 3.76Gyr, the central values of Y and Z are consequently larger by about 7% and 18%, respectively, in the diffusive compared to non-diffusive models of the same age.

As may be seen from Figure 7, Fe contributes as much to the Rosseland opacity as H or He, so that an 18% increase in the abundance of Fe leads to about a 6% increase in Rosseland opacity at a given T and ρ . Furthermore, a given mass of He contributes less to the opacity than the same mass of H (because H and He contributions to the opacity come mainly from their free electrons); with the result that, as Y increases, the opacity decreases. The increase of He abundance reduces from 6% to 5% the increase in opacity, at given T and ρ , caused by the 18% increase of Fe abundance. The effect may be seen just before the appearance of convective cores in the left-hand panel of Figure 6, where the opacity per gram is approximately 4% larger in the diffusive, than in the non-diffusive, models (at $m_r/M_* = 0.038$)⁴. After the appearance of the convective core (right-hand panel), the opacity outside the core is still larger in the diffusive, than in the non-diffusive, models but structural changes wipe out the opacity differences inside the core itself.

The differences in chemical composition, and hence in opacity, appear to be the main cause of the structural differences between the models with, and without, diffusion. The most evident difference is the convective core that appears shortly after 3.76 Gyr in the diffusive models, but not in the non-diffusive one. In the bottom row of panels in Figure 6 is plotted, as a function of the fractional mass, $\nabla_{\text{rad}} - \nabla_{\text{ad}}$, where (from Cox 1968, Eq. 23.171):

$$\nabla_{\text{rad}} = d \ln T / d \ln P = \frac{3}{16\pi acG} \frac{P}{T^4} \frac{\kappa L_r}{m_r}. \quad (3)$$

According to Eq. (2.5) and (2.8) of Stein (1966), one may expect the product T^3/ρ to be approximately constant: this is seen in Figure 8 to hold reasonably well in both the diffusive and non-diffusive models. The P/T^4 term then varies as μ^{-1} and so decreases as Y increases. (For instance, Y increases over time from 0.53 to 0.61 at $m_r/M_* = 0.038$ in the non-diffusive model.) The increasing Y also causes a decrease in the opacity, as may be seen in Fig. 6. At a given m_r ,

⁴At a given m_r/M_* , the T and ρ are not exactly the same in the three models because of structural differences, which explains why the opacity increase is 4% in the models while it is 5% at given T and ρ .

the ratio L_r/m_r increases with time until hydrogen is exhausted. Thus, there are two partially cancelling effects in $\kappa L_r/m_r$ which, however, turns out to increase with time (see Fig. 9).

At 3.76 Gyr, the expression $\kappa L_r/m_r$ is 10% larger in the diffusive, than in the non-diffusive, model, of which 4% comes from the larger κ , and 6% is due to the larger value of L_r/m_r in the diffusive model. At that phase, it is apparent that $\nabla_{\text{rad}} - \nabla_{\text{ad}}$ is close to zero, especially in the case of the diffusive models. For them, $d \ln T / d \ln P$ continues to increase and a convective core appears. However, the central region of the non-diffusive model remains radiative. The reason for this difference is, then, that the small metallicity-induced opacity enhancement in the central region of the 1.1 M_\odot model with diffusion is large enough for a convective core to appear in this model (but not in the one without diffusion) before the opacity is reduced too much by the increasing He abundance.

In the preceding discussion, we implicitly used Schwarzschild’s stability criterion, although the calculations were done using the Ledoux stability criterion. The use of the latter rather than the former has only a moderate effect on the size of the convective core. The main effect of the Ledoux criterion is to temporarily transform a convection zone into a semiconvection zone. Semiconvection then mixes He, however, thereby eliminating the μ gradient and the Schwarzschild criterion is recovered over most of the convective core (as may be seen in Figure 6). There remains an extension of about 20% of the convective core caused by semiconvection. However, the total size of the convective core and of its semiconvective extension approximately equals the size of the convective core that would be obtained if the Schwarzschild criterion were used instead of the Ledoux criterion (since $\nabla_{\text{rad}} = \nabla_{\text{ad}}$ approximately at the outer boundary of the semiconvective core; see the lower part of Fig. 6). Note that allowing for the diffusion of the metals leads to another 15–20% increase in the size of the core (compare the core mass in the model with the diffusion of He only to that obtained when the diffusion of metals is also treated).

4. Isochrones

The interpolation code described by Bergbusch & Vandenberg (1992) has been used to generate isochrones for ages from 3.5 to 10 Gyr from both the non-diffusive and diffusive grids of evolutionary tracks. Figure 10 illustrates several of the computed isochrones and shows that, at the same age, the diffusive isochrones have cooler turnoffs, fainter subgiant branches, and bluer giant branches than those which neglect gravitational settling and radiative accelerations — even when both sets of models are precisely normalized to the Sun, as indicated. (In order to satisfy the solar constraint, the diffusive models required a higher value of the mixing-length parameter, which is the main cause of the differences between the *dashed* and *solid curves* at the base of the red-giant branch. See §2 and Table 1)

A more interesting and informative comparison of the isochrones is given in Figure 11. In this case, isochrones from the non-diffusive and diffusive grids are plotted that resemble each

other most closely; i.e., they predict very similar turnoff and subgiant luminosities. Allowance for diffusive processes clearly leads to a 5–7% reduction in age at a given turnoff luminosity (over the age range considered), which is considerably less than the 10–12% reduction that is predicted by models for extreme Population II stars (see VandenBerg et al. 2002). However, the latter models were constructed for the *same* initial helium and heavy-element abundances, whereas the present computations have assumed *different* initial values of Y and Z in order that both the non-diffusive and diffusive models for $1.0 M_{\odot}$ satisfy the solar constraint. It is, in fact, the differences in the assumed chemistry of the respective Standard Solar Models that have compensated for nearly half of the expected effects of diffusion on predicted turnoff luminosity–age relations.

Fig. 11 also shows that atomic diffusion has important ramifications for the morphology of isochrones in the vicinity of the turnoff. In particular, the “hook” feature in the youngest isochrones, which traces the rapid contraction phase that occurs at central H exhaustion in those stars that have convective cores during their main–sequence phase, is displaced to somewhat higher luminosities and cooler temperatures when diffusive processes are treated. (Note that the largest differences between the *solid* and *dashed* loci occur when they deviate to higher values of T_{eff} just prior to the beginning of the subgiant stage.) This is very reminiscent of the effects of convective core overshooting. (Indeed, as already mentioned, diffusive models *do* have enlarged convective cores and, as shown in the next section, they provide a much improved match to the CMD of the ≈ 4 Gyr, open cluster M 67, as compared with those that neglect diffusion and convective overshooting.)

Moreover, convective cores clearly persist to fainter absolute magnitudes when diffusion is treated: at the same turnoff luminosity, the diffusive isochrone for 5.6 Gyr possesses a small “hook” feature, while none is present in the 6.0 Gyr non-diffusive isochrone. In fact, the maximum age for which an observed CMD is expected to show a gap near the main–sequence turnoff is ≈ 5.7 Gyr if diffusion is treated, and ≈ 4.8 Gyr if diffusion is neglected. Thus, open clusters with ages between approximately 4.8 and 5.7 Gyr have the potential to further test the effects of diffusion physics in the central regions of stars. (This difference in age is a consequence of the fact that the stellar mass marking the transition between tracks that have convective cores throughout the main–sequence phase, and those which do not, is lower for the diffusive models — $1.097 M_{\odot}$ versus $1.14 M_{\odot}$, see § 3.3.)

As shown in Figs. 10 and 11, the blueward hooks in the oldest isochrones that possess such features (in both the diffusive and non-diffusive grids) have small “kinks” at their faint ends. They arise because of the sudden change in the track morphology at the transition mass. Consider, for instance, the tracks plotted in Figure 12 for 1.095 and $1.097 M_{\odot}$ stars, in the case that diffusion is treated. The *filled circles* indicate where the predicted age is 5.55 Gyr on both tracks and it is clear that an isochrone for this age (and similar ages) must undergo a redward jog between these two points.

5. Application to M 67 and NGC 188

In their presentation of improved $UBVI$ photometry for M 67, Meynet et al. (1993) concluded that “none of the current isochrones fit our data consistently”. The morphology of the main-sequence turnoff and the luminosity of the gap at the turnoff were especially problematic for the models that they considered. Since that study was published, the evidence has become overwhelming that there is significant overshooting beyond the boundaries of convective cores as determined from the Schwarzschild criterion (e.g., Meynet et al. 1993; Demarque et al. 1994; Nordstroem et al. 1997; Schroder et al. 1997; Rosvick & Vandenberg 1998). There has also been widespread agreement that the amount of overshooting is less in stars that are just above the mass marking the transition between stars that possess convective cores on the main-sequence and those which do not, than in stars of appreciably higher mass. In particular, the extent of core overshooting appears to be equivalent to ≈ 0.1 pressure scale heights in the turnoff stars of M 67, whereas something closer to $0.25H_P$ is typically found in studies of much younger open clusters (see the aforementioned papers, as well as Sarajedini et al. 1999). However, given the results described in the previous section, is it possible that diffusive isochrones can provide a good fit to the M 67 CMD without requiring *any* convective overshooting?

To answer this question, we have transposed our isochrones to the observed plane using the semi-empirical color- T_{eff} relations described by Vandenberg & Clem (2003), and performed a main-sequence fit of the Montgomery et al. (1993) CMD for M 67 to the isochrones. The assumption of a solar metallicity is within the 1σ uncertainty of most estimates of the cluster $[m/H]$ value. For instance, Sarajedini et al. (1999) concluded that M 67 has $[m/H] = -0.05 \pm 0.08$ from their consideration of the best available determinations prior to their paper, and the latest high-resolution spectroscopic study that we are aware of has obtained $[m/H] = -0.03 \pm 0.03$ (Tautvaišienė et al. 2000). Moreover, the reddening that is obtained from the Schlegel et al. (1998) dust maps, $E(B - V) = 0.038$, is in very good agreement with independent estimates (see the Sarajedini et al. study). Consequently, the distance modulus that is derived from a main-sequence fit to the isochrones should be quite accurate (under these assumptions).

The left-hand panel of Figure 13 shows how well the non-diffusive isochrones are able to reproduce the M 67 CMD. The derived distance modulus is $(m - M)_V = 9.70$ and the age of the isochrone that provides the best match to the cluster subgiants is 3.8 Gyr. M 67 is known to have a high binary fraction — Montgomery et al. (1993) have estimated that at least 63% of the cluster stars are binaries — which certainly complicates the interpretation of the data. For instance, a large fraction of the group of stars just above the gap (at $M_V \approx 3.1$) are likely to be binaries given that such a large number of stars at nearly the same color on the subgiant branch is contrary to the predictions of stellar evolutionary theory. The fact that they are displaced by 0.5–0.75 mag above the main-sequence population is consistent with many of them being nearly equal-mass binaries (see the simulated CMDs reported by Carraro et al. 1994).

In most respects, the isochrone fits the observed CMD rather well. However, the predicted

location of the termination of the main-sequence, and hence of the gap just above it, are somewhat too faint. As illustrated in the right-hand panel of Figure 13, this difficulty can be alleviated to some extent if the observations are fitted to diffusive isochrones. In this case, a slightly smaller distance modulus, $(m - M)_V = 9.67$, is obtained from the main-sequence fit, and the inferred age is also slightly less (3.7 Gyr). (If the same distance modulus were adopted as in the left-hand panel, the inferred age would be closer to 3.6 Gyr.) Although the comparison between theory and observation is still not completely satisfactory (the isochrone appears to be a bit too red at $3.6 \lesssim M_V \lesssim 4.1$), it does represent a significant improvement over that given in the left-hand panel. (Even the predicted location of the base of the red-giant branch is much more consistent with that observed.)

To reinforce this conclusion, we show in Figure 14 the same isochrones that appear in the previous figure with crosses plotted along them at $0.01 M_\odot$ intervals. The density of the crosses gives a good indication of the expected variation in the numbers of stars along the two isochrones. For instance, the blueward hook should manifest itself as a gap in the distribution of turnoff stars, and relatively few stars should be found on the subgiant branch because the rate of evolution is fast, and the variation of mass with evolutionary state is low, in this phase. The vertical line bounded by short horizontal lines just to the right of each isochrone indicates the observed location of the gap in M67 (from Fig. 13). Given that considerably fewer stars are predicted to be found in the magnitude range encompassed by the observed gap in the right-hand panel than in the left-hand panel, the diffusive isochrone clearly provides the best fit to the observations. (Whether or not the model fit could be further improved by assuming a small amount of convective overshooting is difficult to say in view of the high fraction of binary stars and significant field star contamination.)

It is, of course, very comforting that the diffusive models appear to be the most realistic ones since it is well known that such calculations are favored from solar oscillation studies — e.g., Christensen-Dalsgaard et al. (1993); Richard et al. (1996). At this time, we can only speculate that errors in the adopted color– T_{eff} relations or the assumed abundances (perhaps of helium) are responsible for the small color offset between the models and observations at $M_V \sim 3.8$.

As noted above, a solar abundance, open cluster having an age between 4.8 and 5.7 Gyr would provide a good test of the models since it is only the diffusive models in this age range that predict the existence of a main-sequence gap. Unfortunately, only a few old open clusters have been identified to date, and it seems unlikely that any of them have the right age to provide such a test. Perhaps the best candidate is NGC 188, but it appears to be too old by ~ 0.5 –1 Gyr. In the left-hand panel of Figure 15, a main-sequence fit of the Sarajedini et al. (1999) CMD for NGC 188 to the non-diffusive isochrones yields $(m - M)_V = 11.40$ and an age of 6.9 Gyr, on the assumption of $E(B - V) = 0.087$ (Schlegel et al. 1998). As noted by Sarajedini et al., this reddening estimate is in good agreement with independent determinations, and there is considerable spectroscopic support for a metallicity near solar. They adopted $[m/H] = -0.04 \pm 0.05$, but more recent work (Randich et al. 2003; Worthey & Jowett 2003) favors $[Fe/H] \gtrsim 0.0$. The isochrone provides quite a satisfactory fit to the observations, except at the base of the red-giant branch.

If the same reddening is assumed, a main-sequence fit of the photometry to the diffusive isochrones also yields $(m - M)_V = 11.40$, but an age of 6.4 Gyr. As shown in the right-hand panel of Figure 15, this isochrone provides a very good match to the observed CMD, including the lower giant branch. Thus, by treating gravitational settling and radiative accelerations, the inferred age of NGC 188 has been reduced by $\approx 7\%$. There is no indication of a gap in the observed CMD, nor is any predicted, but it is curious that the majority of the stars at $3.8 \lesssim M_V \lesssim 4.2$ are redder than the isochrone (in both panels), giving one the impression that the best-fitting isochrone should have a small redward jog in this magnitude range.

6. Conclusions

Since the Sun is used to normalize convection parameters and initial abundances, one could have imagined that, in solar metallicity clusters having ages similar to that of the Sun, models with diffusion would lead to the same age and the same CMD properties as models without diffusion. The variations of α and initial abundances required to fit the Sun in the diffusion model reproduce the same $1.0 M_\odot$ star at the same age and the two sets of models could be expected to do the same for star clusters. Reality turns out to be more complex. For age determinations, partial cancellation effectively occurs, but the shapes of isochrones turn out to be quite different near the turnoff. Both the normalization to solar abundances and the additional gravitational settling in the central regions of stars work together to cause an 18% increase in the central metallicity. This increases the size of the convective core in stars of 1.09 to $1.3 M_\odot$ (see §3.3) which, in turn, modifies the morphologies of isochrones (see §4) around the solar age.

An important consequence of the changes in the shapes of isochrones that arise when diffusive processes are treated is that it is possible to match the CMD of M 67 (including the luminosity of the gap near the turnoff) without having to assume an *ad hoc* amount of convective core overshooting: a diffusive isochrone for 3.7 Gyr does a remarkably good job of matching the cluster observations. The other significant result of this investigation, as far as isochrones are concerned, is that a gap near the turnoff is predicted to persist in open clusters up to an age of ≈ 5.7 Gyr by the diffusive models, whereas the limiting age is closer to 4.8 Gyr if diffusion is not treated. It would be important to have detailed observations of the fiducial sequences for such clusters as those identified by Friel et al. (2002) to test this prediction. Unfortunately, NGC 188 appears to be too old to do this, given that our best estimate of its age is 6.4 Gyr based on the diffusive isochrones (which, incidently, provide a superb match to the observed CMD).

The predicted surface abundance variations among near turnoff stars turn out to be limited to approximately 0.1 dex in M 67 and 0.07 dex in NGC 188 (see §3.1). Most elements heavier than Si have their surface abundances modified by g_{rad} but no large overabundances are expected. While not negligible, such variations are not easy to detect at the present time. The existing Li/Be measurements in a few stars of M 67 (see §3.2) suggest that another process may be required to reduce the Li abundance (see Sills & Deliyannis 2000) though the Be/Li trend obtained with models

including all aspects of atomic diffusion is very different from the trend obtained by these authors. With improved observations this becomes a test of various turbulent models and will be further discussed in a paper in preparation on LiBeB abundances in cluster and field main–sequence stars.

This work has been supported by Operating Grants to G. M. and to D. A. V. from the Natural Sciences and Engineering Research Council of Canada. We thank the Réseau Québécois de Calcul de Haute Performance (RQCHP) for providing us with the computational resources required for this work.

REFERENCES

- Bahcall, J. N., Pinsonneault, M. H., & Wasserburg, G. J. 1995, *Rev. Mod. Phys.*, 67, 781
- Balachandran, S. 1995, *ApJ*, 446, 203
- Barrett, E. A., Boesgaard, A. M., King, J. R., & Deliyannis, C. P. 2001, in *American Astronomical Society Meeting 199*, #57.10, Vol. 199, 0–+
- Bergbusch, P. A. & Vandenberg, D. A. 1992, *ApJS*, 81, 163
- Brun, A. S., Turck-Chieze, S., & Zahn, J. P. 1999, *ApJ*, 525, 1032
- Caputo, F., Chieffi, A., Castellani, V., Collados, M., Roger, C. M., & Paez, E. 1990, *AJ*, 99, 261
- Carraro, G., Chiosi, C., Bressan, A., & Bertelli, G. 1994, *A&AS*, 103, 375
- Christensen-Dalsgaard, J., Proffitt, C. R., & Thompson, M. J. 1993, *ApJ*, 403, 75
- Cox, J. P. 1968, *Principles of stellar structure - Vol.1: Physical principles; Vol.2: Applications to stars* (New York: Gordon and Breach, 1968)
- Demarque, P., Sarajedini, A., & Guo, X.-J. 1994, *ApJ*, 426, 165
- Dinescu, D. I., Girard, T. M., van Altena, W. F., Yang, T., & Lee, Y. 1996, *AJ*, 111, 1205
- Eggen, O. J. & Sandage, A. R. 1969, *ApJ*, 158, 669
- Friel, E. D., Janes, K. A., Tavares, M., Scott, J., Katsanis, R., Lotz, J., Hong, L., & Miller, N. 2002, *AJ*, 124, 2693
- Gonzalez, J.-F., LeBlanc, F., Artru, M.-C., & Michaud, G. 1995, *A&A*, 297, 223
- Guenther, D. B., Kim, Y.-C., & Demarque, P. 1996, *ApJ*, 463, 382
- Guzik, J. A. & Cox, A. N. 1992, *ApJ*, 386, 729
- . 1993, *ApJ*, 411, 394
- Hobbs, L. M. & Thorburn, J. A. 1991, *ApJ*, 375, 116
- Hobbs, L. M., Thorburn, J. A., & Rodriguez-Bell, T. 1990, *AJ*, 100, 710
- Iben, I. J. 1965, *ApJ*, 142, 1447
- Kaluzny, J. 1990, *Acta Astronomica*, 40, 61
- Kato, S. 1966, *PASJ*, 18, 374
- Krishna Swamy, K. S. 1966, *ApJ*, 145, 174

- Langer, N., El Eid, M. F., & Fricke, K. J. 1985, *A&A*, 145, 179
- LeBlanc, F., Michaud, G., & Richer, J. 2000, *ApJ*, 538, 876
- Maeder, A. 1997, *A&A*, 321, 134
- Martín, E. L., Basri, G., Pavlenko, Y., & Lyubchik, Y. 2002, *ApJ*, 579, 437
- McClure, R. D. & Twarog, B. A. 1977, *ApJ*, 214, 111
- Meynet, G., Mermilliod, J.-C., & Maeder, A. 1993, *A&AS*, 98, 477
- Michaud, G. 1977, *Nat*, 266, 433
- Michaud, G. & Proffitt, C. R. 1993, in *Inside the Stars*, IAU COLLOQUIUM 137, Vienna, April 1992, ASP Conference Series, 40, ed. W. W. Weiss & A. Baglin (San Francisco: ASP), 246
- Montgomery, K. A., Marschall, L. A., & Janes, K. A. 1993, *AJ*, 106, 181
- Nordstroem, B., Andersen, J., & Andersen, M. I. 1997, *A&A*, 322, 460
- Paquette, C., Pelletier, C., Fontaine, G., & Michaud, G. 1986, *ApJS*, 61, 177
- Piau, L. & Turck-Chièze, S. 2002, *ApJ*, 566, 419
- Platais, I., Kozhurina-Platais, V., Mathieu, R. D., Girard, T. M., & van Altena, W. F. 2003, *AJ*, in print
- Proffitt, C. R. 1994, *ApJ*, 425, 849
- Proffitt, C. R. & Michaud, G. 1989, *ApJ*, 346, 976
- Randich, S., Primas, F., Pasquini, L., & Pallavicini, R. 2002, *A&A*, 387, 222
- Randich, S., Sestito, P., & Pallavicini, R. 2003, *A&A*, 399, 133
- Richard, O., Michaud, G., & Richer, J. 2001, *ApJ*, 558, 377
- Richard, O., Michaud, G., Richer, J., Turcotte, S., Turck-Chieze, S., & Vandenberg, D. A. 2002, *ApJ*, 568, 979
- Richard, O., Vauclair, S., Charbonnel, C., & Dziembowski, W. A. 1996, *A&A*, 312, 1000
- Richer, J., Michaud, G., Rogers, F., Iglesias, C., Turcotte, S., & LeBlanc, F. 1998, *ApJ*, 492, 833
- Rosvick, J. M. & Vandenberg, D. A. 1998, *AJ*, 115, 1516
- Sandage, A. 1962, *ApJ*, 135, 349
- Sarajedini, A., von Hippel, T., Kozhurina-Platais, V., & Demarque, P. 1999, *AJ*, 118, 2894

- Schlegel, D. J., Finkbeiner, D. P., & Davis, M. 1998, *ApJ*, 500, 525
- Schroder, K., Pols, O. R., & Eggleton, P. P. 1997, *MNRAS*, 285, 696
- Sills, A. & Deliyannis, C. P. 2000, *ApJ*, 544, 944
- Stein, R. F. 1966, in *Proceedings of an International Conference, held at the Goddard Space Flight Center, Greenbelt, November 13-15, 1963*, New York: Plenum Press, 1966, edited by Stein, R.F.; Cameron, A.G.W., ed. R. F. Stein & A. G. W. Cameron, 3
- Tautvaišiene, G., Edvardsson, B., Tuominen, I., & Ilyin, I. 2000, *A&A*, 360, 499
- Turcotte, S., Richer, J., Michaud, G., Iglesias, C., & Rogers, F. 1998, *ApJ*, 504, 539
- VandenBerg, D. A. & Clem, J. L. 2003, *AJ*, 126, 778
- VandenBerg, D. A., Richard, O., Michaud, G., & Richer, J. 2002, *ApJ*, 571, 487
- Worthey, G. & Jowett, K. J. 2003, *PASP*, 115, 96

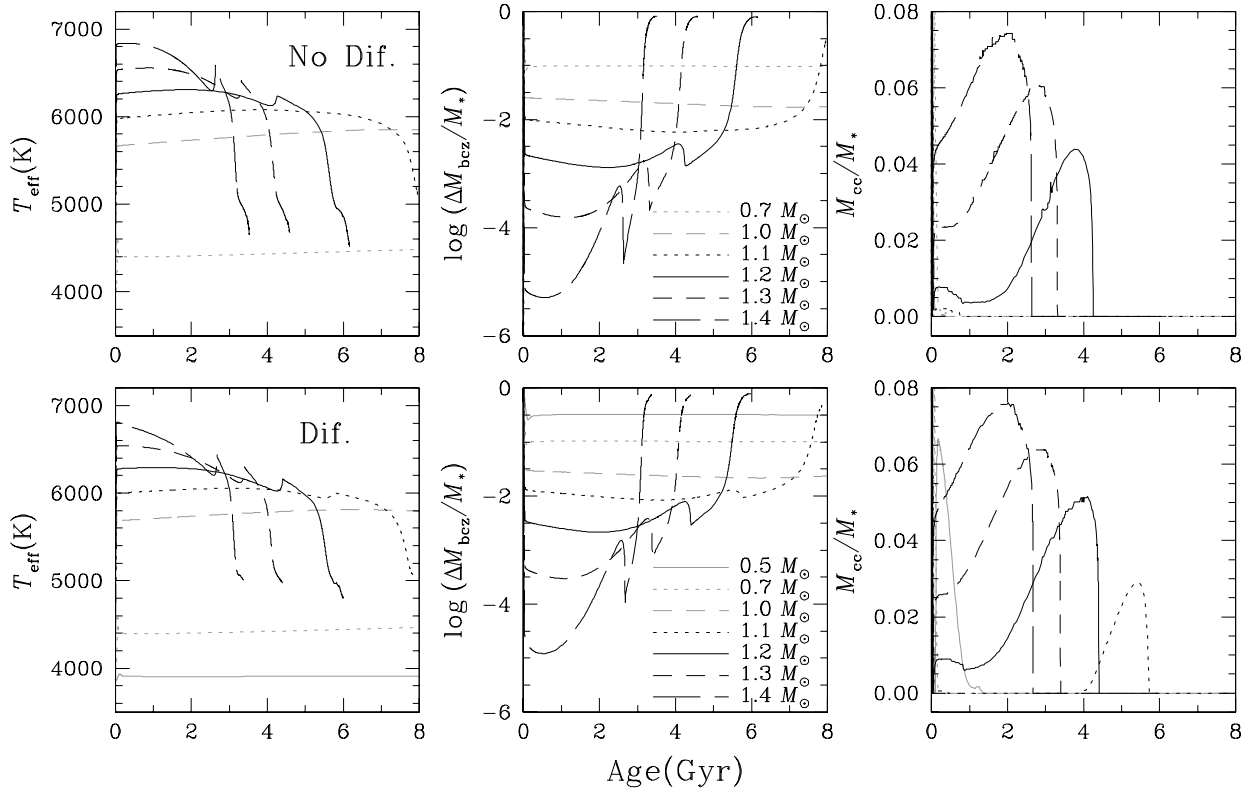


Fig. 1.— Properties of a few of the calculated models without diffusion (top row) and with atomic diffusion (bottom row) as a function of time. Surface abundances are mainly determined by diffusion processes occurring immediately below the surface convection zone (center panels). The mass of the central convective core is shown in the right-hand panels. While the 1.1 M_{\odot} model with diffusion has a central convective core, that without diffusion does not.

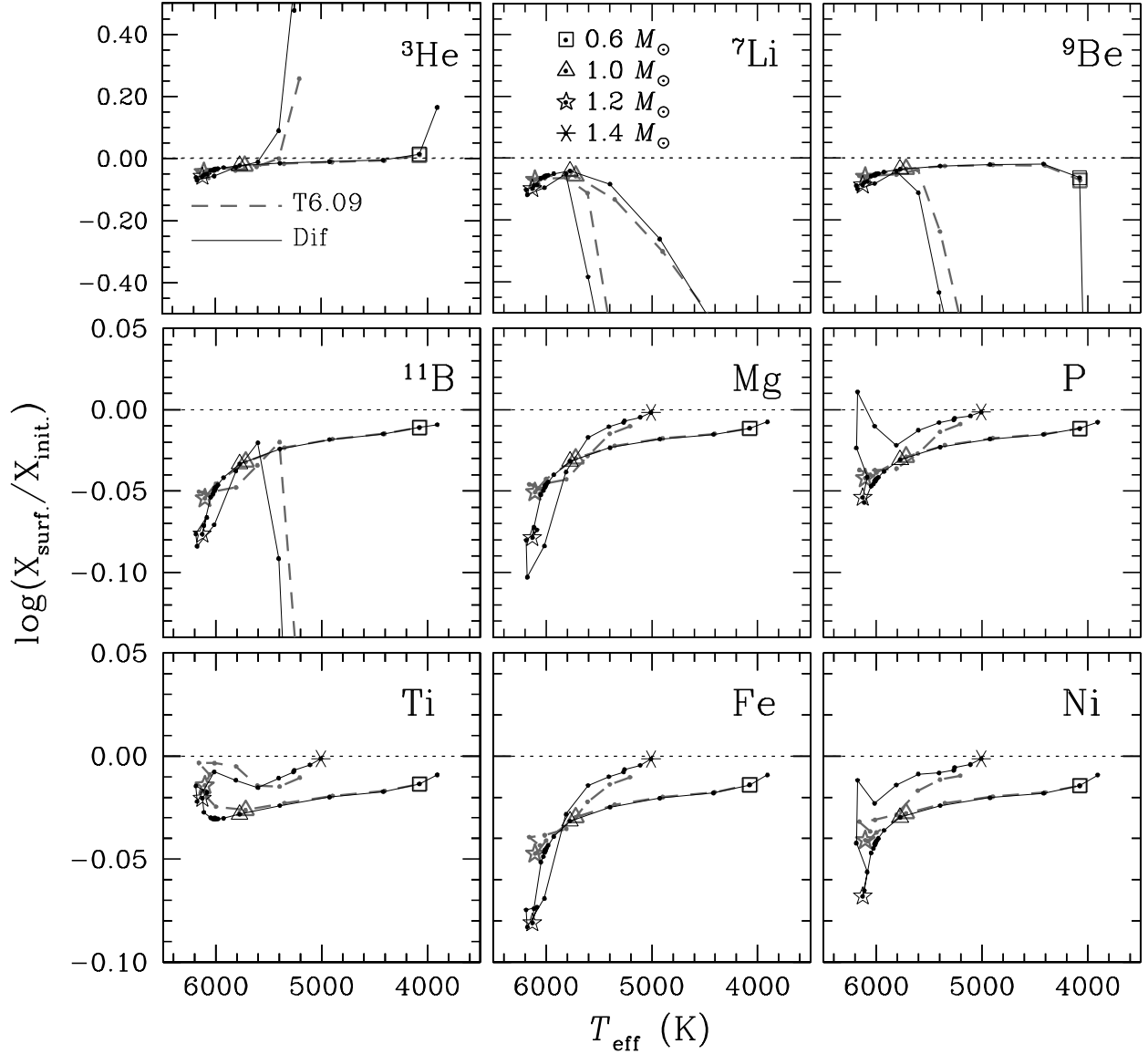


Fig. 2.— Chemical abundances at the surface of solar metallicity stars at 3.7 Gyr in models with atomic diffusion and in those with T6.09 turbulence. Such surface abundance isochrones were calculated for 28 species, but only representative ones are shown. The smallest mass star is always at the extreme right of each curve. Special characters are used for a few stellar masses and they are identified on the figure.

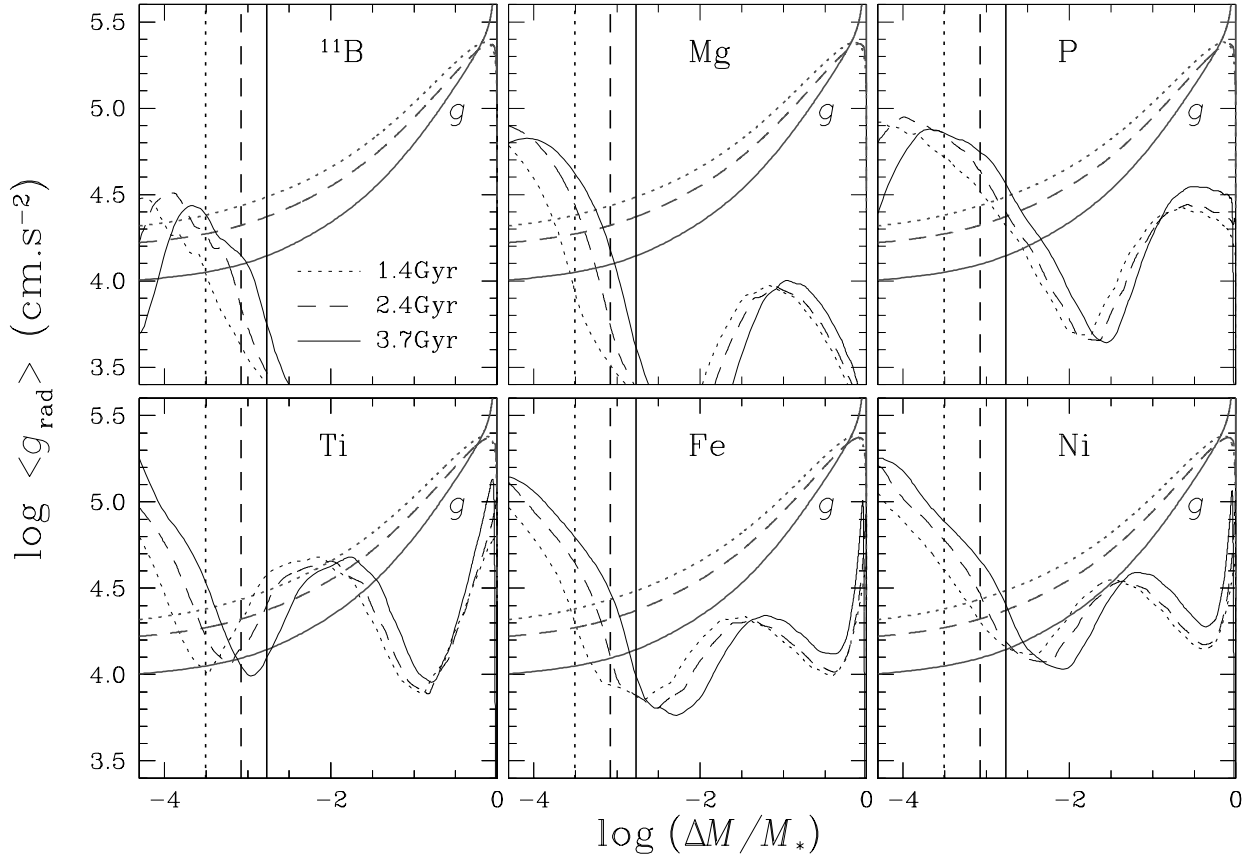


Fig. 3.— Radiative accelerations in a $1.3 M_{\odot}$ solar metallicity star at 1.4, 2.4, and 3.7 Gyr. The bottom of the surface convection zone at each epoch is indicated by a vertical line of the same type. Gravity (g) is plotted in each panel of the figure. The g_{rad} of Li and Be are not shown because they are always smaller than that of B below the surface convection zone and so do not have a significant impact on Li and Be abundances.

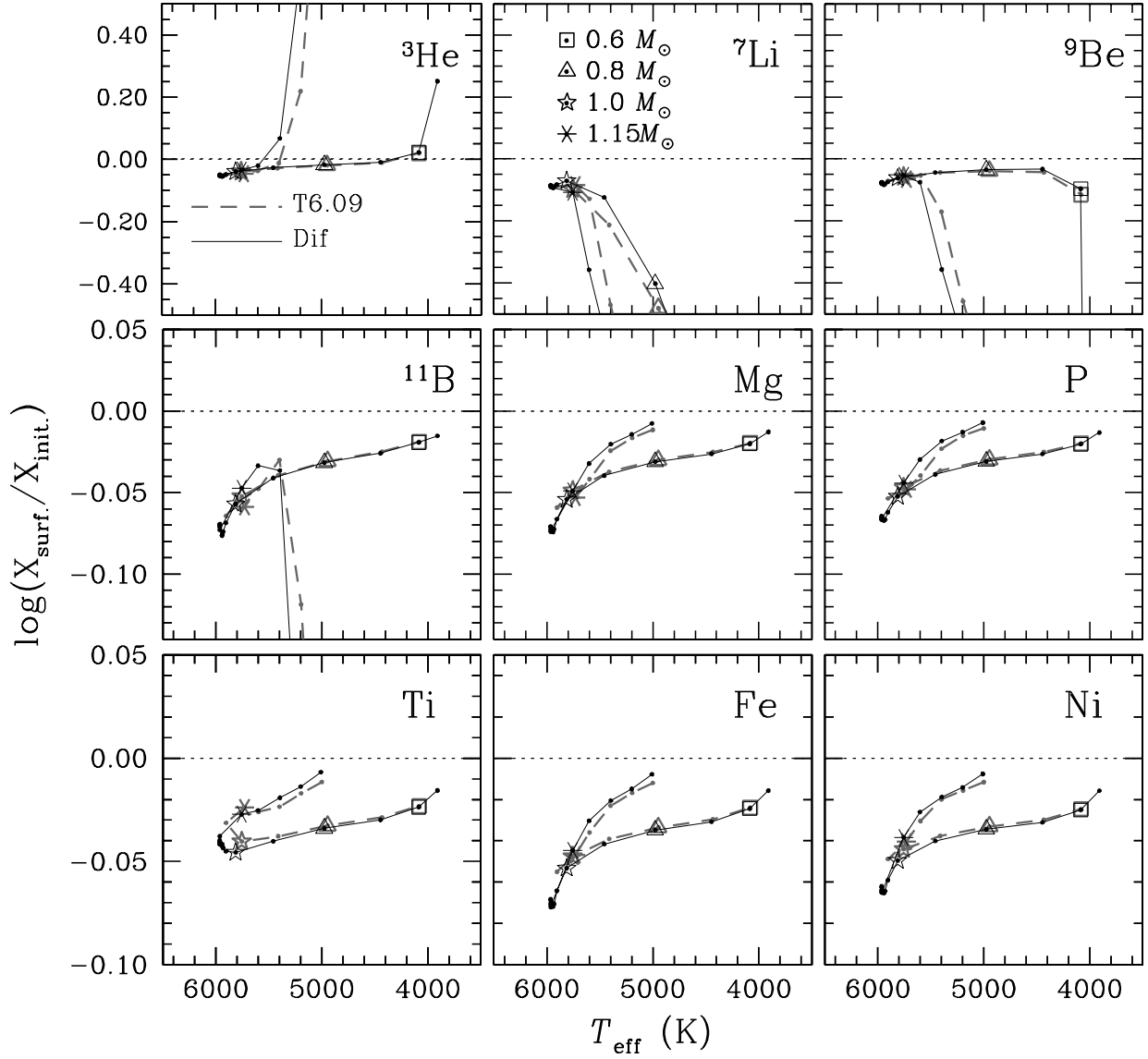


Fig. 4.— Same as in Fig. 2 but at 6.4 Gyr as appropriate for NGC 188.

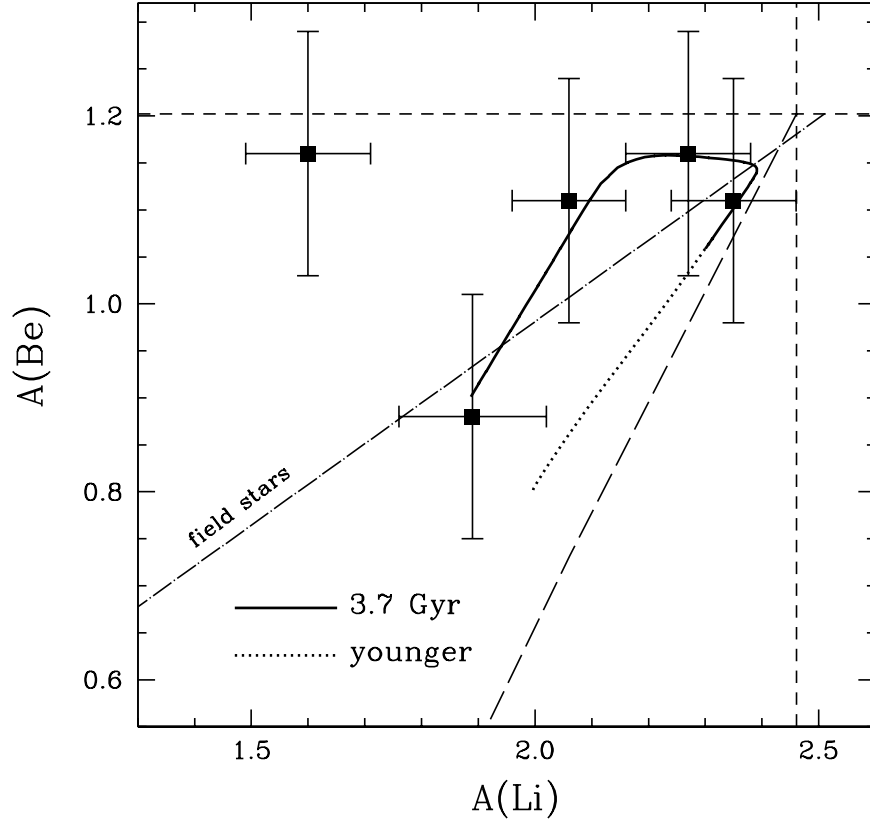


Fig. 5.— Isochrone of the lithium to beryllium abundance ratio in M67 stars with $T_{\text{eff}} \geq 5500$ K from models with atomic diffusion (solid curves of Li and Be on Fig. 2). The left segment of the solid curve represents stars starting on the subgiant branch while the right segment indicates main-sequence stars and the nearly horizontal one denotes stars at turnoff. The dotted part of the curve was occupied at earlier times by stars that have now evolved to the subgiant or giant evolutionary state. The horizontal and vertical dashed lines indicate the initial values used in the calculations. The data points are from Randich et al. (2002) and their quoted error bars are plotted. For comparison purposes, the long dashed curve gives the evaluation of Li/Be due to atomic diffusion by Sills & Deliyannis (2000) (adjusted to have the same zero age main-sequence values as we used), while the dot dashed curve is their fit to the observed Li/Be ratio in field stars.

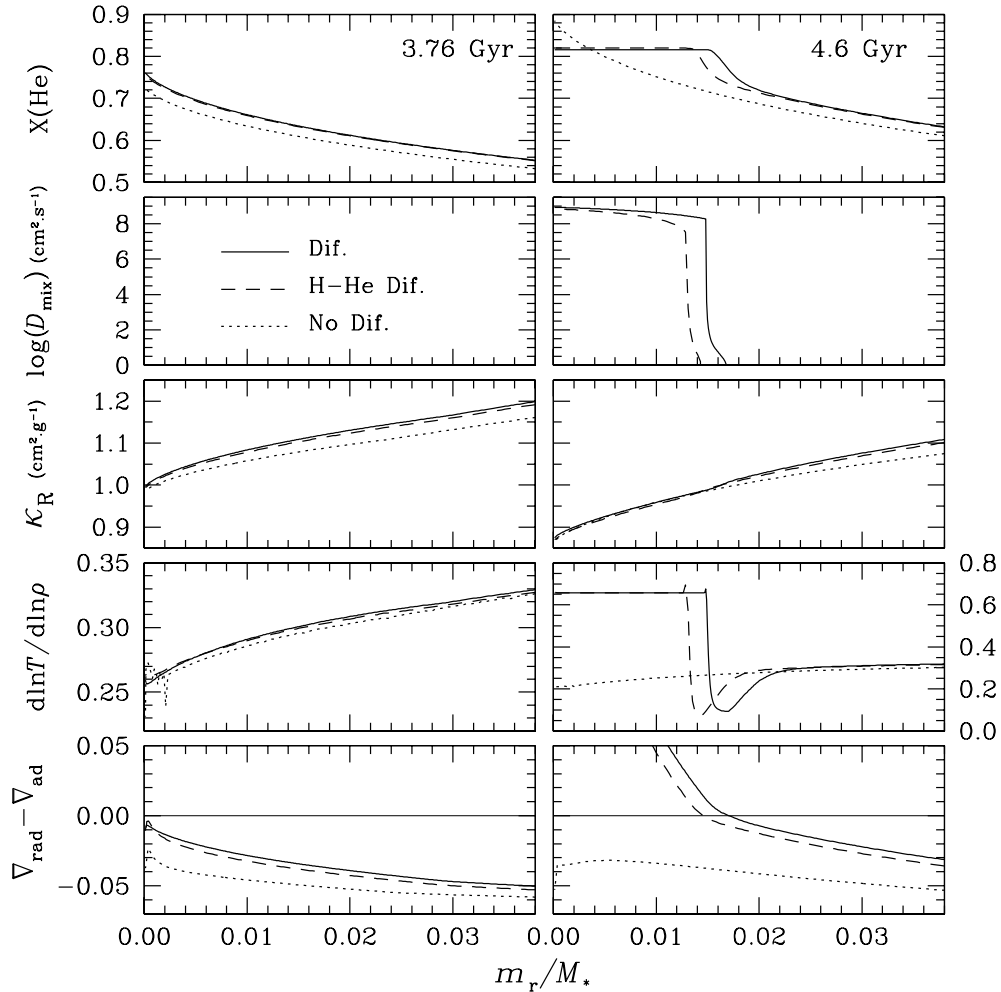


Fig. 6.— Important properties of three $1.10 M_{\odot}$ models at $\simeq 3.76$ Gyr (left panels), just before the appearance of the central convective cores in the models with diffusion. The *solid line* is the model with atomic diffusion of all species, the *dashed line* is the model with H-He diffusion but no diffusion of metals, while the *dotted line* is the model without diffusion. In the panels to the right are shown the same properties when the convective cores are well developed in the diffusive models (at 4.6 Gyr). The same scales are used for the right- and left-hand panels, except for the $d \ln T / d \ln \rho$ panel. The mixing coefficient, D_{mix} , is caused by convection over the m_r / M_* interval where D_{mix} is nearly horizontal and equal to $10^8 \text{ cm}^2 \text{ s}^{-1}$. At the upper boundary of the convective core, it drops to $10^2 \text{ cm}^2 \text{ s}^{-1}$ and then continues decreasing in the semiconvection zone. While $X(\text{He})$ is constant in the convective core, there remains a substantial He abundance variation in the semiconvective region. From the plots in the bottom row, one sees that the radiative and adiabatic gradients become equal approximately at the upper boundary of the semiconvective zone, so that using the Schwarzschild, instead of the Ledoux, criterion would actually lead to a larger convective core than the Ledoux criterion used here. It would include both the convective core and its semiconvective extension.

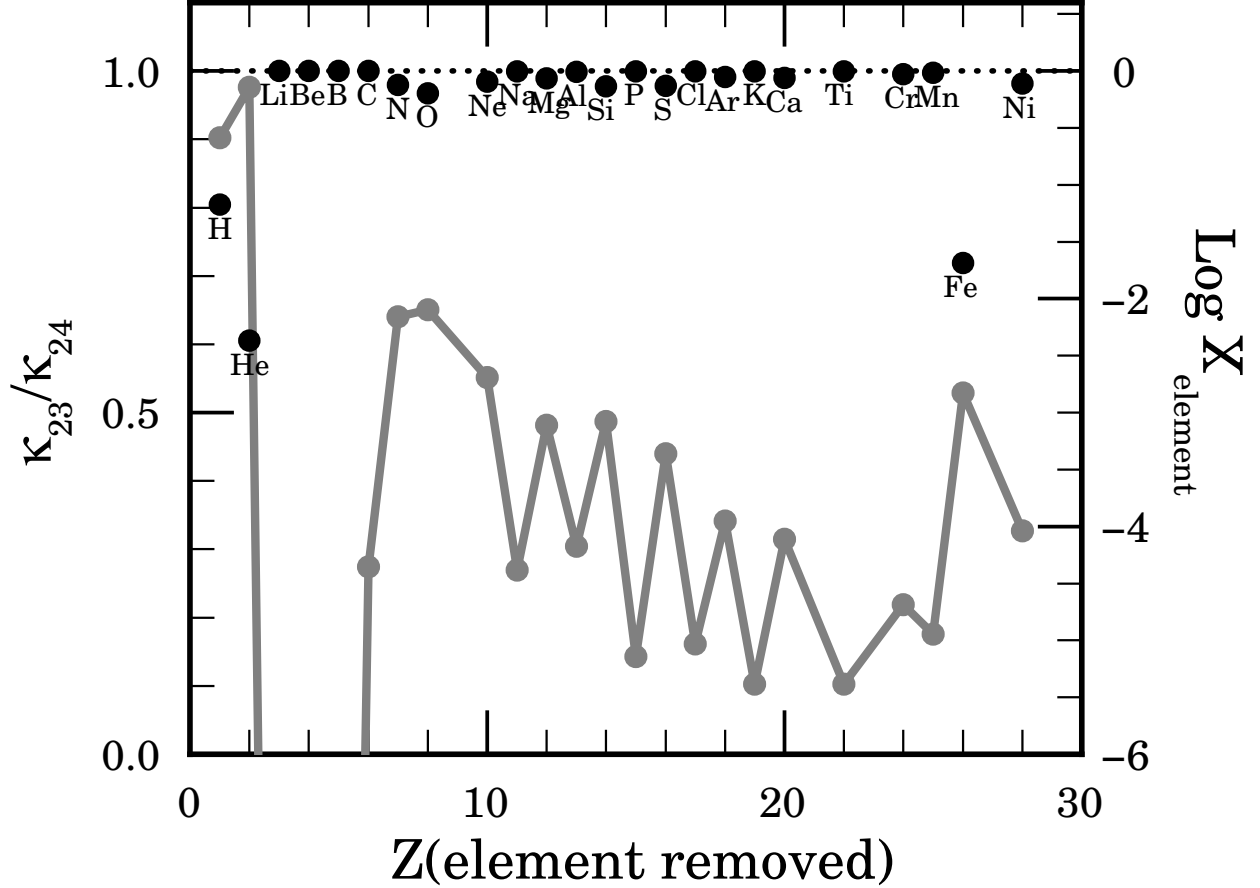


Fig. 7.— Evaluation of the contribution of each element to the Rosseland-averaged opacity in the $1.1 M_{\odot}$ model with diffusion at an age of 4.6 Gyr, just outside of the convective core (near $m_r/M_* \simeq 0.02$, see Fig. 6): the gray line and the right-hand scale give the local mass-fraction abundance of each element. Fe contributes to the opacity as much as H or He, and an increase in the Fe abundance leads to a significant increase in the Rosseland opacity. Since Fe contributes about one-third of the opacity, an 18% increase in the Fe abundance leads to a 6% increase in the opacity. For Fe, which has not lost all of its electrons, the main contribution is from bound-bound and bound-free transitions, while for H and He, the main contribution is from free-free transitions.

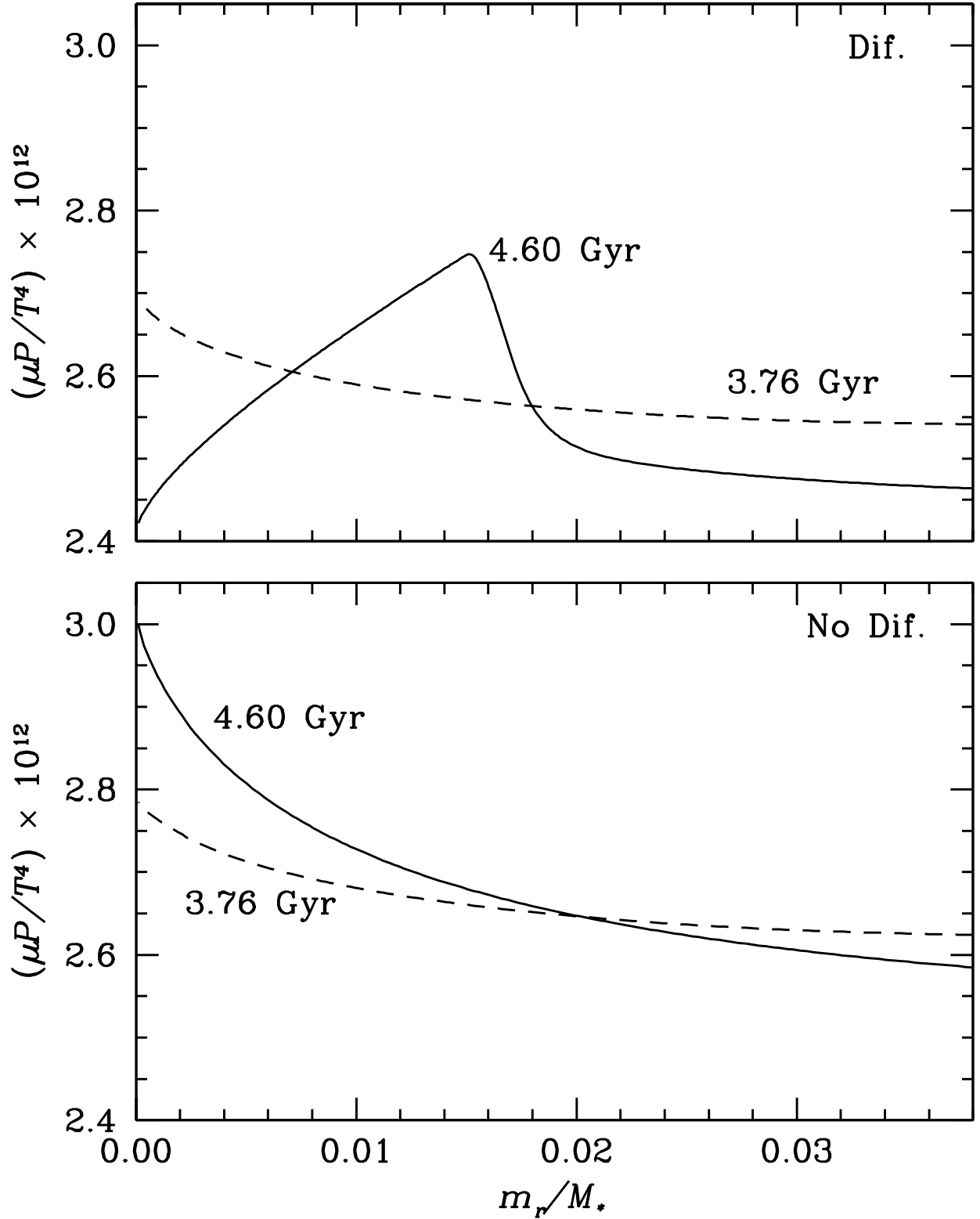


Fig. 8.— The ratio $\rho/T^3 \propto \mu P/T^4$ is approximately constant in both the $1.1 M_\odot$ models with, and without, diffusion and it has close to the same value in both. See the text for a discussion of its role in the appearance of convective cores.

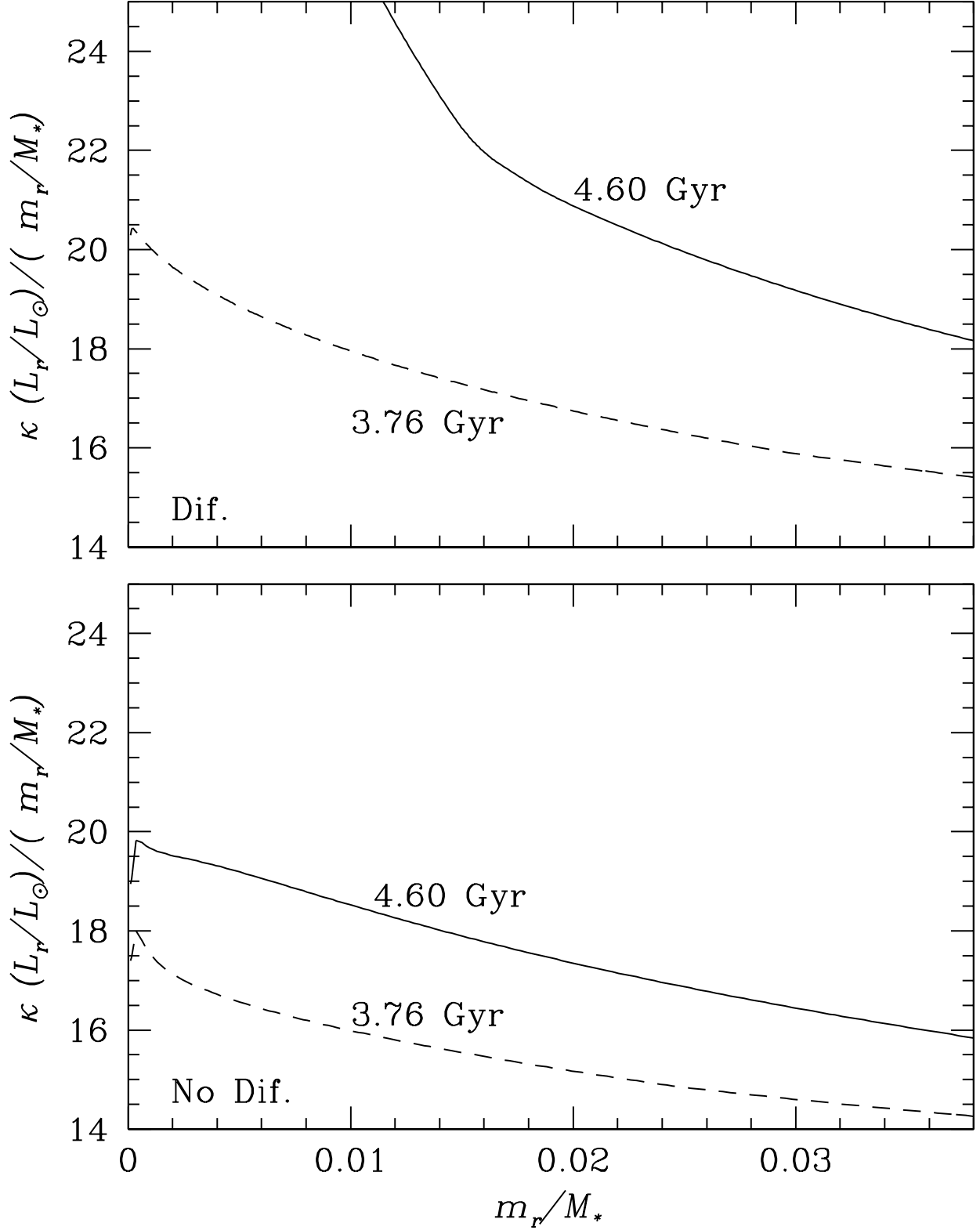


Fig. 9.— The variation of the ratio $\kappa L_r/m_r$ with mass and with age near the centers of the $1.1 M_\odot$ models with, and without, diffusion. Note that this ratio is larger in the model with diffusion at a given age. See the text for a discussion of its role in the appearance of a central convective core.

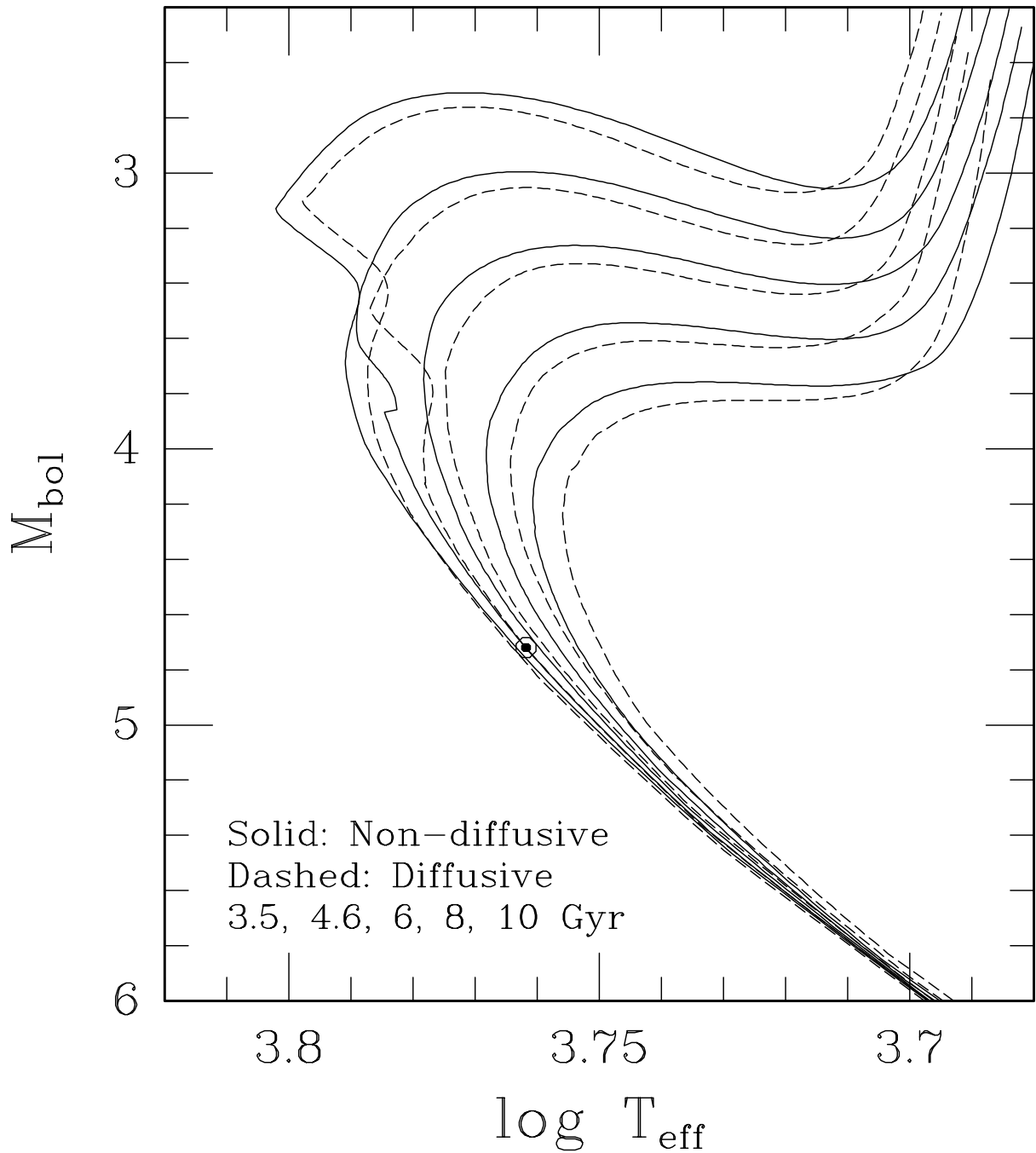


Fig. 10.— Comparison of non-diffusive and diffusive isochrones (*solid* and *dashed* curves, respectively) for $[m/H] = 0.0$ and the indicated ages. The location of the Sun on this diagram is given by the *solar symbol*. To satisfy the solar constraint, the non-diffusive and diffusive isochrones had to be shifted by $\delta \log T_{\text{eff}} = -0.0022$ and -0.0012 , respectively).

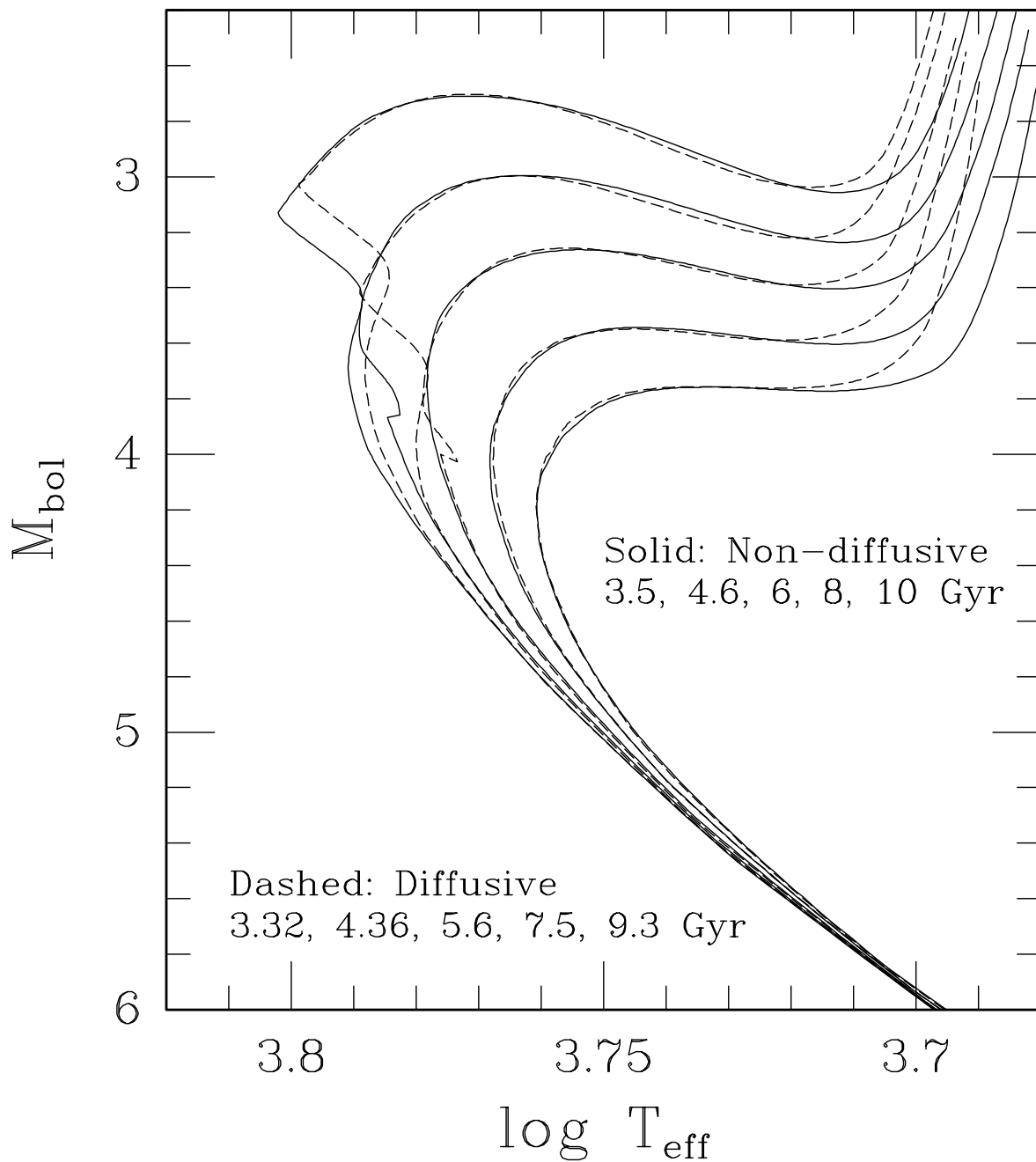


Fig. 11.— As in the previous figure, except that diffusive isochrones have been selected so as to provide the closest match to the subgiant branches and/or the turnoffs of the non-diffusive isochrones. The ages of the former are $\sim 5 - 7\%$ less than the latter. Note that, in order to match the main-sequence locations of the non-diffusive isochrones, the diffusive isochrones were shifted by small amounts ranging from $\delta \log T_{\text{eff}} = -0.001$ to $+0.002$ over the age range considered.

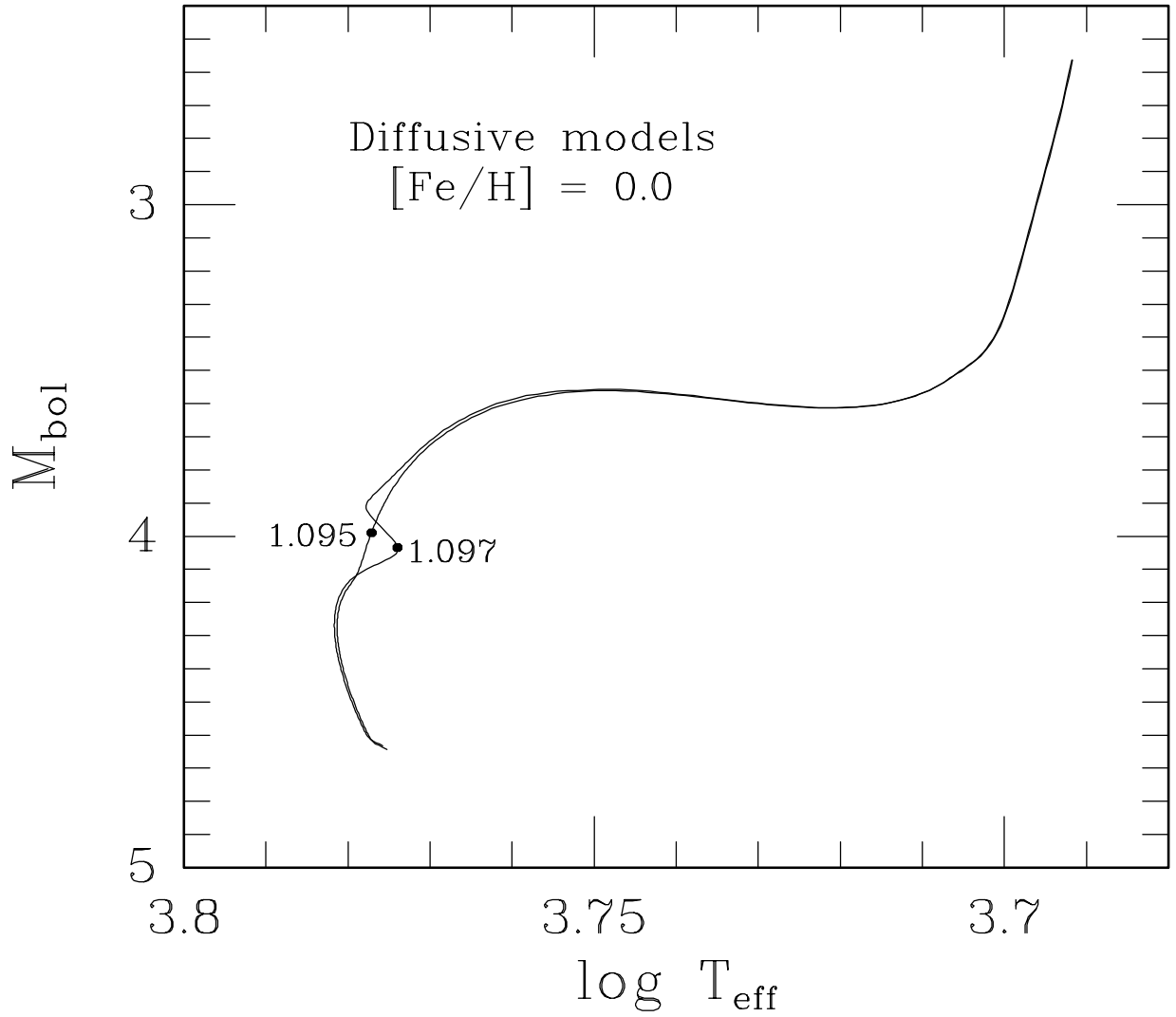


Fig. 12.— Evolutionary tracks from the zero-age main sequence to the lower giant branch for 1.095 and 1.097 M_{\odot} and the solar metallicity, to show the very rapid development of the convective hook feature. Diffusive processes are treated in these computations.

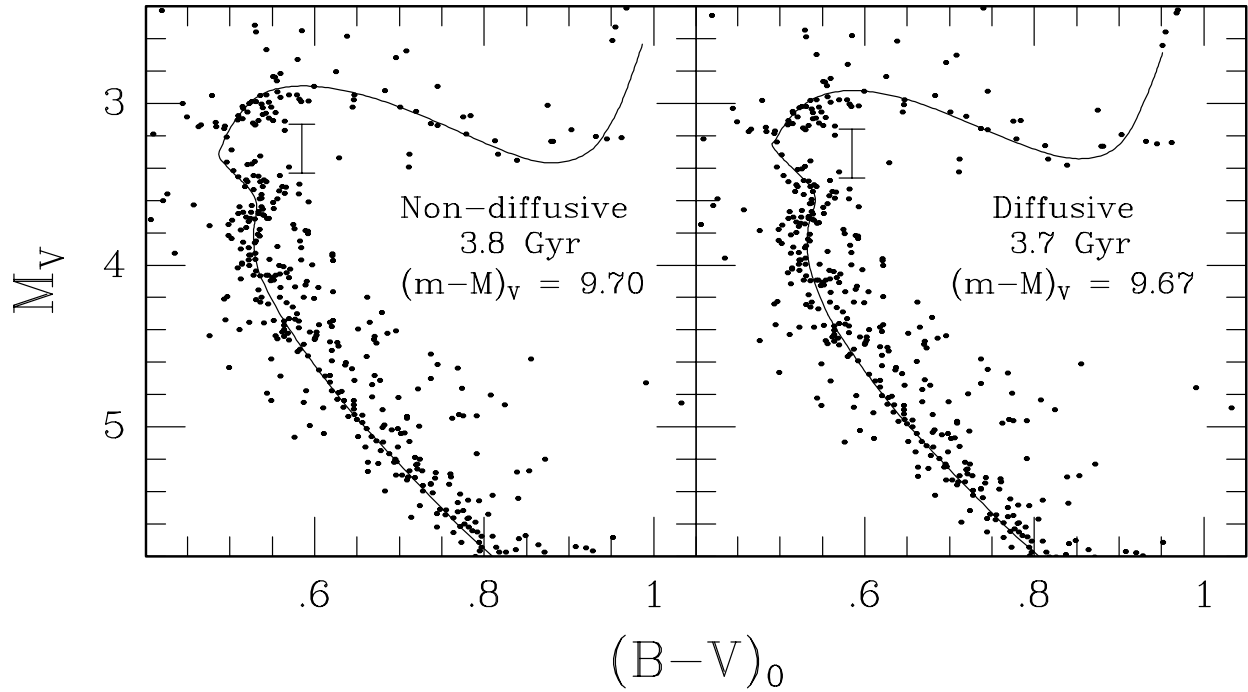


Fig. 13.— Main-sequence fits of the Montgomery et al. (1993) CMD for M67 to the non-diffusive and diffusive isochrones that provide the best match to the cluster’s subgiant branch. The reddening is assumed to be $E(B - V) = 0.038$ mag (Schlegel et al. 1998), and the derived distance modulus is $(m - M)_V = 9.70$ and 9.67 , respectively. Note the differences in the vicinity of the turnoff, which indicate a clear preference for the diffusive isochrone. Our estimate of the luminosity spanned by the gap in M67 is indicated by the vertical line bounded by short horizontal lines: it is used in the next plot.

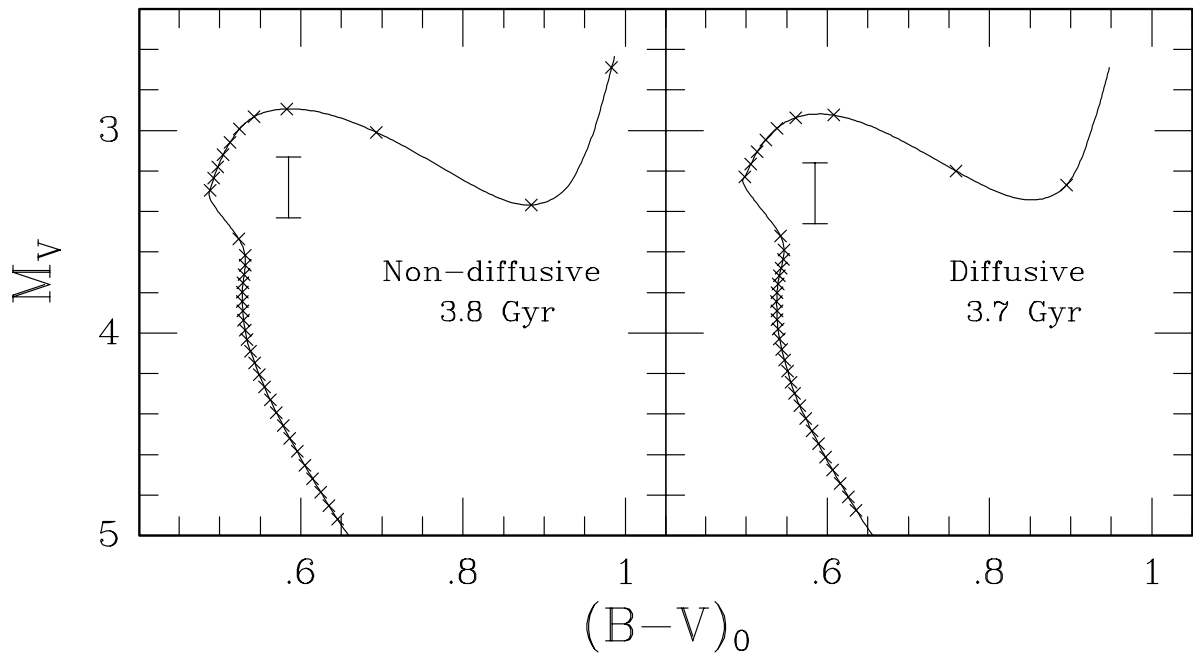


Fig. 14.— The isochrones from the previous figure are plotted with crosses superposed at $0.01 M_\odot$ mass intervals. To first approximation, the same number of cluster stars is expected between adjacent crosses. The vertical line bounded by short horizontal lines indicates the magnitude range spanned by the gap in M67. It is to be compared with the location of the predicted gap (as defined by the blue hook) in both panels.

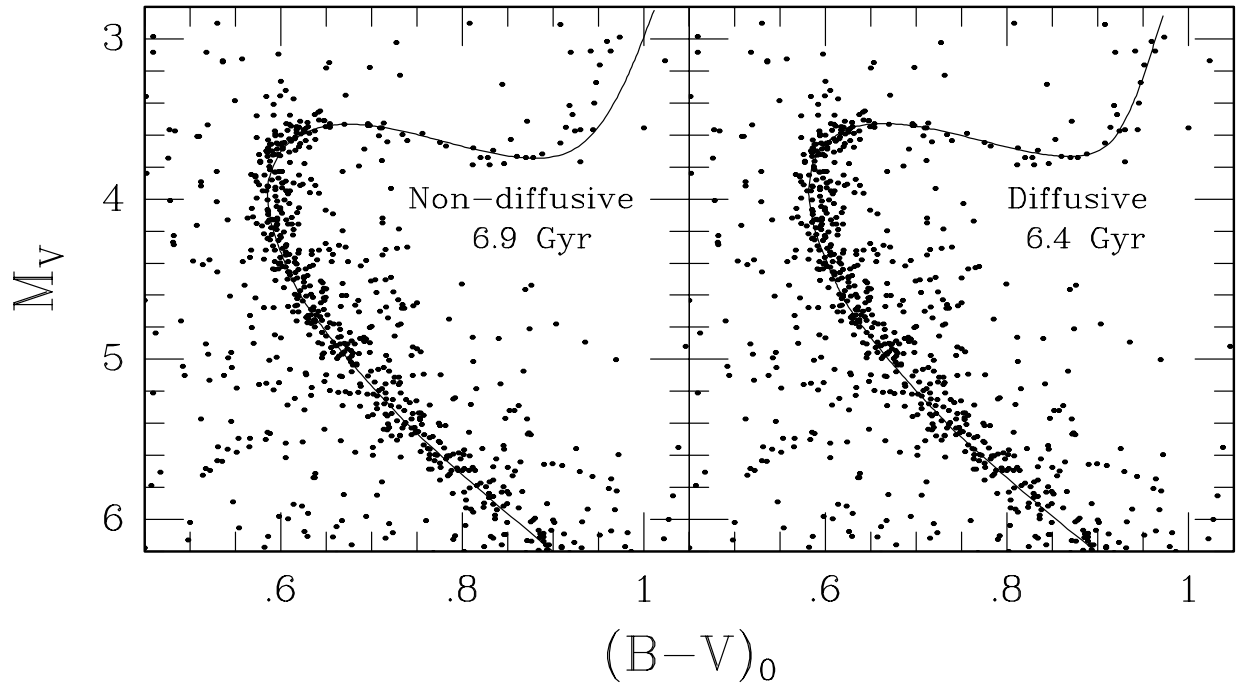


Fig. 15.— Similar to Figure 13, except that the CMD of NGC 188 (Sarajedini et al. 1999) is fitted to non-diffusive and diffusive isochrones that provide the best match to the cluster’s subgiant branch, if it is assumed that $E(B - V) = 0.087$ (Schlegel et al. 1998). In both cases, the derived distance modulus is $(m - M)_V = 11.40$.

Table 1. Computed Solar Metallicity Tracks

Z_0	Y_0	α_{MLT}	Boundary ^a condition	Atomic diffusion	Turbulence	L/L_\odot ^b	R/R_\odot ^c
0.01750	0.26811	1.94646	KS	No	No	0.999	0.996
0.01999	0.27769	2.09635	KS	yes	No	1.002	1.002
0.01999	0.27769	2.09635	KS	yes	T6.09 ^d	1.001	1.002

^a KS: Krishna-Swamy

^b $L_\odot = 3.86 \times 10^{33}$ erg.s⁻¹

^c $R_\odot = 6.9599 \times 10^{10}$ cm

^d See Richard et al. (2002)